Padimi et al., Materials Letters 278 (2020) 128371, https://doi.org/10.1016/j.matlet.2020.128371

Corresponding author: V. Padimi, *E-mail:* venkateshp.mme@gmail.com

Visualisation of stabilising particles at the gas-solid interface of metal foams

V. Pamidi [a,⇑], G. Mohan Muralikrishna [a], S. Bhogi [a,b], K. Georgy [a], B. Muduli [a], F. García-Moreno [c], M. Mukherjee [a]

[a] *Department of Metallurgical and Materials Engineering, Indian Institute of Technology Madras, Chennai 600036, India*
[b] *Department of Basic Science and Humanities, GMR Institute of Technology, Rajam 532127, India*
[c] *Institute of Applied Materials, Helmholtz-Zentrum Berlin für Materialien und Energie, Hahn-Meitner-Platz 1, 14109 Berlin, Germany*

Abstract

In this article, we demonstrate a technique to visualise the stabilising particles at the gas-solid interface of metal foams by employing *metallographic etching*. This technique is easy to perform and can be applied on a relatively large sample size. The particles present at the gas-solid interface of five different types of foams were investigated. Information on the type of particles and the particle coverage could be obtained from this study.

1. Introduction

Closed-cell metal foams produced by the melt route and pow- der metallurgy (PM) route are mainly stabilised by solid particles such as SiC [1], TiB_2 [2], Al_2O_3 [3–5], $MgAl_2O_4$ [6], etc. These particles stabilise liquid films either by segregating at the gas-liquid interface and thereby modifying the curvature of the gas-liquid interfaces of the film and/or by forming mechanical bridges across it [4,7]. These particles also increase melt viscosity, which in turn reduces drainage and thereby improves stability [8].

The visualisation of particles in solid metal foams is crucial in understanding stabilisation mechanisms. Haibel et al. used micro computed tomography (mCT) on solid foams containing SiC particles using a synchrotron X-ray source to visualise particles at the gas-solid interfaces [9]. Dudka et al. employed focused ion beam (FIB) tomography on Al foam produced by PM route to visualise oxide particle network inside cell wall [5]. Synchrotron-based X-ray imaging was used for in-situ observation of SiC particles inside liquid Al film [10]. Transmission electron microscope (TEM) was also used for the visualisation of particles [3]. The main advantages of these techniques are the visualisation of particles in 3D (FIB), visualisation of a large sample size in 3D (mCT) and visualisation of nanometer-sized particles along with crystal structure information (TEM). However, these techniques also have some limitations: FIB tomography and TEM are time consuming and suitable only for small sample volume, synchrotron-based mCT is not readily accessible and usually not suitable for particles smaller than 10 mm. Scanning electron microscope (SEM) can be used to visualise micrometer- to sub-micrometer-sized particles over a large gas- solid interfacial area [3,10,11]. However, because of the presence of an oxide layer at the gas-solid interface, many particles are partially or fully hidden [10]. Although Babcsán et al. adopted a polishing technique to remove the oxide layer to facilitate visualisation of particles, only one cell wall can be probed at a time in this technique [3].

To overcome the aforementioned challenges, we adopted the standard *metallographic etching* technique to reveal the particles at the gas-solid interface of solid aluminium foams. Later, SEM was used to visualise these particles. It is an easy-to-perform and relatively quick technique to gather data over a large sample size.

2. Materials and methods

Five different types of foams were analysed. The foams were produced by melt injection technique (MIT) [12,13], Alcan process [3], Alporas process [14] and PM route [15]. In MIT foams, bubbles are created by air entrainment in Al melt (MIT_Al foam) and Al- TiB_2 melt (MIT_Al-TiB_2 foam), whereas bubbles are injected in Al-20vol.%SiC melt in the case of Alcan foam. TiH_2 blowing agent was used to produce bubbles in Alporas and PM foams. The processing details of all the foams are provided in the Supplementary materials. X-ray tomography and image analysis were performed to visualise and analyse the structure of the foams. For metallographic analysis, one sample was extracted from each type of foam. Samples were cold mounted and ground using 600 grit size emery paper. After that, etching was performed on MIT foams with a mixture of 25 ml methanol, 25 ml HCl, 25 ml HNO_3 and 2 drops of HF solution for about 10 s, whereas other foams were etched with Keller's Etch [16]. The type of etchant for each foam was chosen based on some preliminary studies. Etching was performed by immersing the already-ground sample (ground surface facing downward) in the etchant and applying gentle shaking for about 10 s. Microstructures were obtained using SEM (FEI-Quanta 400) equipped with energy dispersive spectroscopy (EDS), both before and after etching.

3. Results and discussion

The macrostructure of the solidified foams can be seen in Fig. 1. Considering the standard deviation, the D_{mean} values of all the foams are not significantly different from each other. Although some structural differences can be observed, it is evident that all the samples have a typical foam structure. This automatically implies that all the foams are stabilised.

A comparison between Fig. 2a and b demonstrates how etching can be exploited to reveal the gas-solid interfacial particles that are either partially or fully hidden by an oxide layer. Particles cannot be observed in Fig. 2a as the interface is covered with an oxide layer, whereas they can be seen after etching (Fig. 2b). These particles exhibit faceted morphology, see Fig. 2c. Table 1 indicates them as alumina particles as previously reported elsewhere [12].

The agglomerated particles in Fig. 2d indicate that some of them are partially visible even before etching. This could be because of a relatively thinner oxide layer in those regions. Fig. 2e and f show two morphologically different particles after etching MIT_Al-TiB_2 foam. Table 1 indicates them as TiB_2 (Fig. 2e) and alumina (Fig. 2f) particles, respectively. TiB2 particles were present in the ingot used for foaming whereas the alumina particles formed dur- ing the foaming process [12,13].

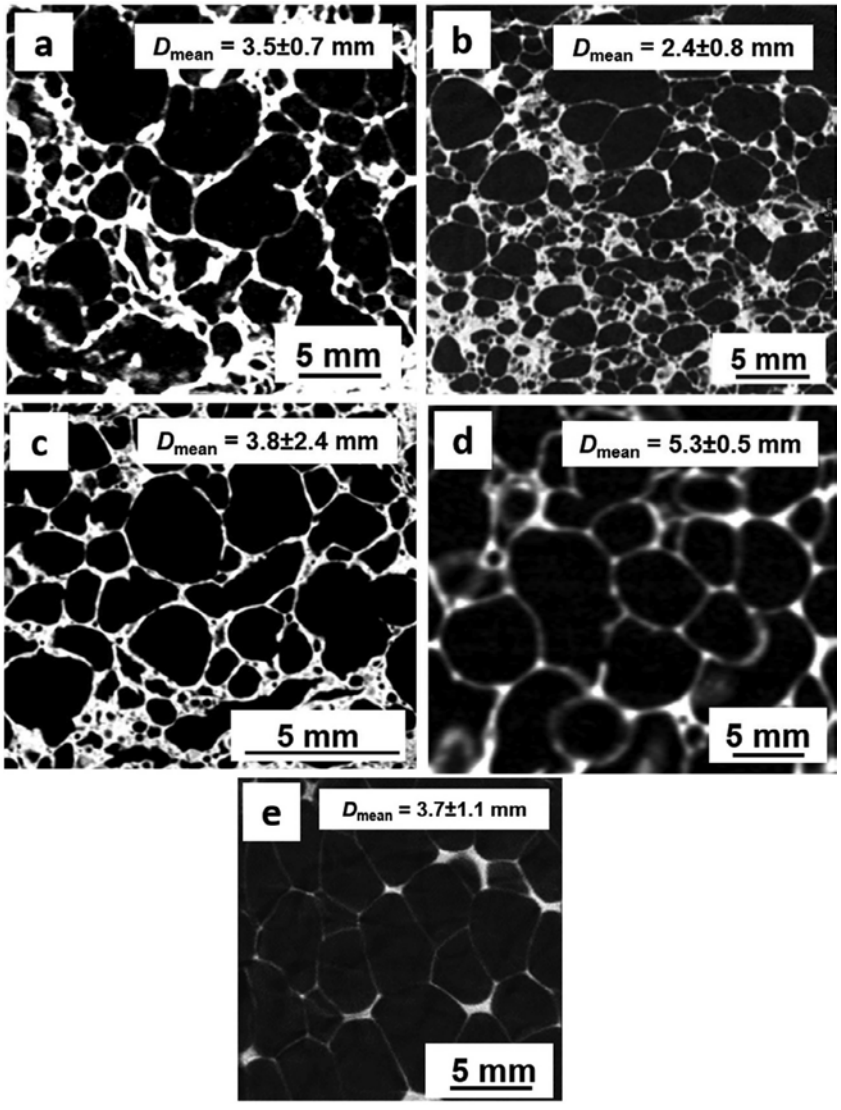

Fig. 1. 2D X-ray tomograms of (a) MIT_Al, (b) MIT_Al-TiB_2, (c) PM, (d) Alporas and (e) Alcan foams. D_{mean} for each foam was determined by fitting their cell size distribution with a log-normal function.

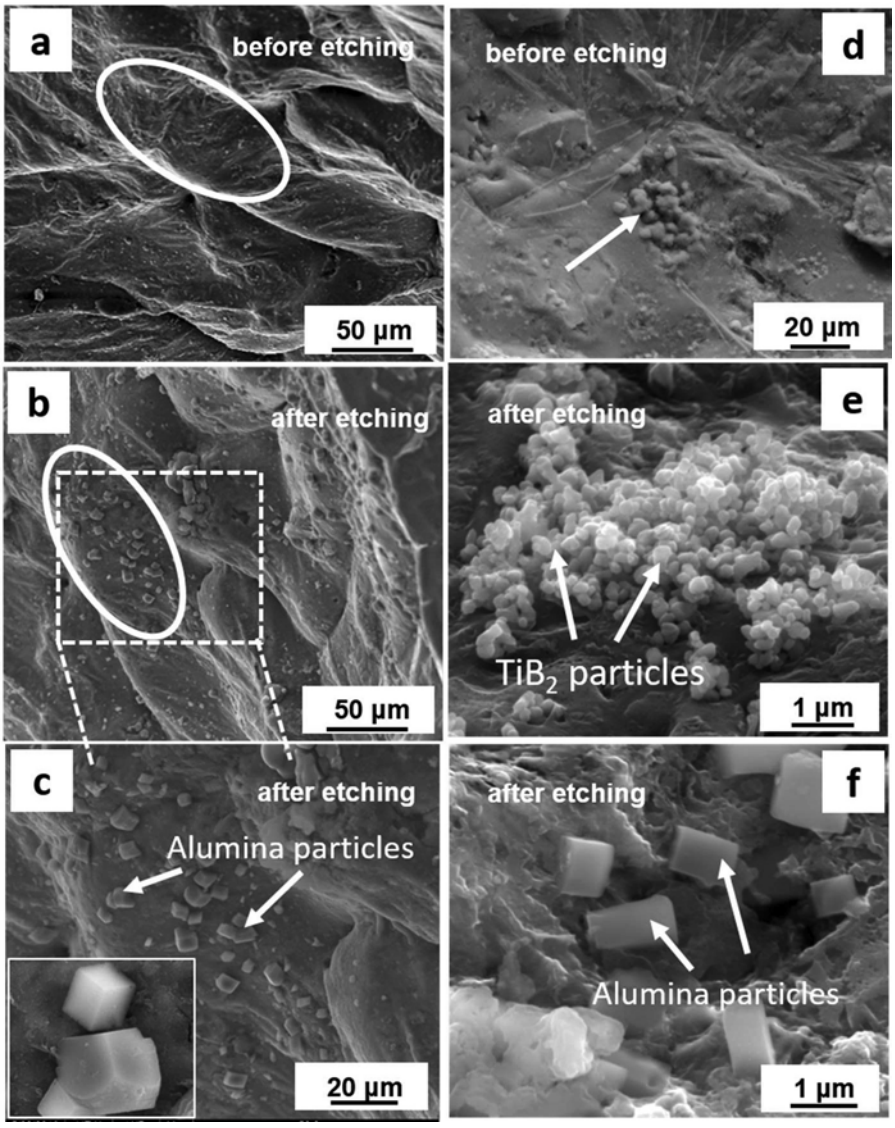

Fig. 2. SEM images (SE mode) of (a-c) MIT_Al foam and (d-f) MIT_Al-TiB_2 foam. Elliptical regions in (a) and (b) correspond to the same area showing no particles and particles, respectively. The inset (width of the image is 10 µm) in (c) shows two particles from where the EDS signals were obtained. Arrow in (d) shows partially visible particles.

Table 1
EDS analysis of the particles from different types of metal foams used in this study. Each value in this table is the average of two measurements. The error indicates standard deviation. All the values are in at.%.

Element	MIT_Al foam	MIT_Al-TiB2 foam		Alcan foam	Alporas foam	PM foam
		Type 1 particles (Fig. 2e)	Type 2 particles (Fig. 2f)			
Al	31.2 ± 10	81.89 ± 1.5	71.7 ± 8.3	31.4 ± 8	82 ± 0.6	73.4 ± 3
O	64.2 ± 10		28.3 ± 8.3	28.5 ± 0.14	14.7 ± 0.6	15.8 ± 2.8
C				34 ± 8.2		
Si				5.5 ± 0.15		9.8 ± 0.02
Mg	4.5 ± 0.4			0.5 ± 0.1		0.9 ± 0.2
Ca					3.4 ± 0.01	
Ti		18.1 ± 1.5				

Before etching no particle can be observed at the gas-solid interface of Alcan type foam, Fig. 3a. The presence of wrinkles (inset of Fig. 3a) confirms that the interface is covered with an oxide layer. Etching removes the oxide layer revealing particles of irregular shape as seen in Fig. 3b. As expected, these particles are SiC as suggested by a high amount of carbon in the EDS signals.
The unetched microstructure of Alporas type foam (Fig. 3c) reveals oxide layer wrinkles and partially visible particles. Whereas, Fig. 3d shows particles revealed after etching. These particles corre- spond to Al-Ca-O phases, see Table 1. The X-ray diffraction (XRD) pattern of the extracted particles from Al-Ca melt suggests that these could be Al_4CaO_7 particles (see Supplementary

4material,

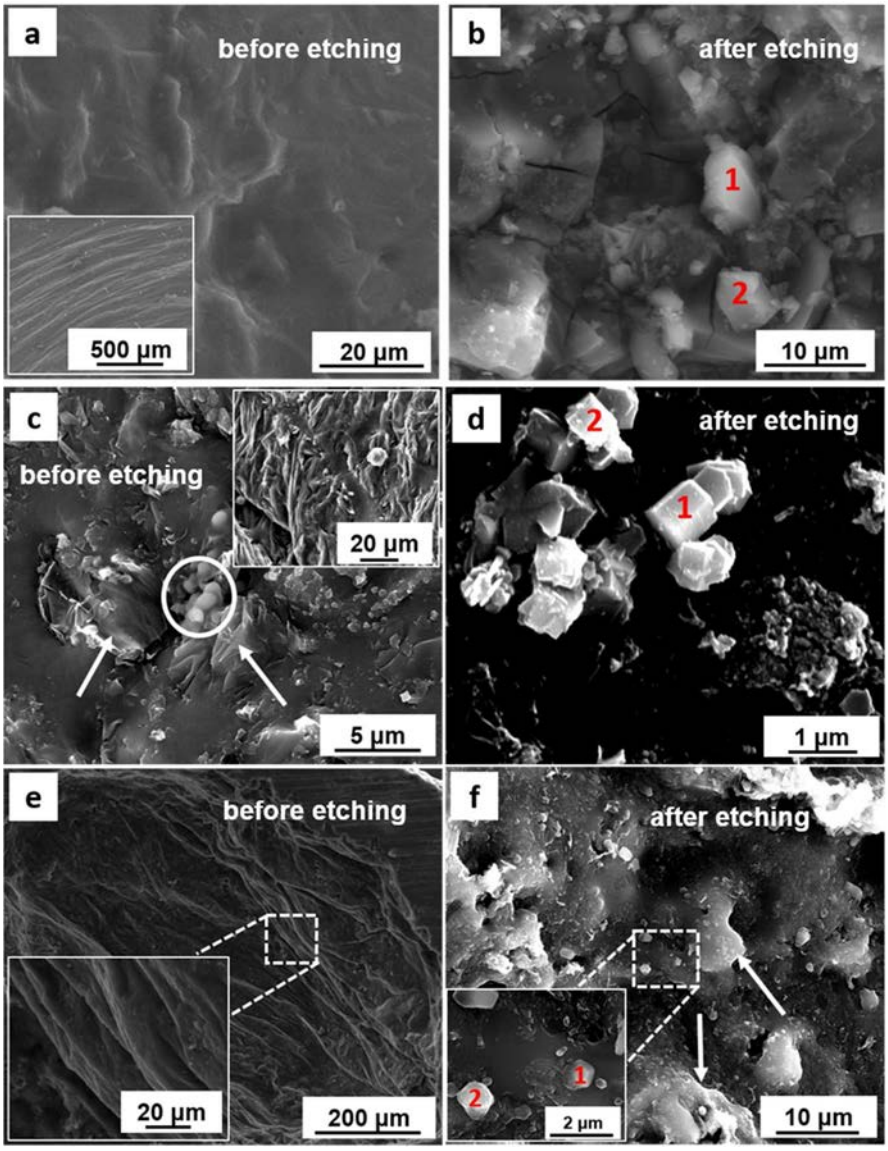

Fig. 3. SEM images (SE mode) of the gas-solid interface of (a, b) Alcan, (c, d) Alporas and (e, f) PM foam. The inset in (a) shows oxide layer wrinkles at the gas–solid interface. The inset in (c) is a low magnification image of the gas-solid interface. The insets in (e) and (f) corresponds to high magnification images of the respective square-marked regions. The circle and arrows in (c) indicate partially visible particles and oxide layer wrinkles, respectively. EDS signals were obtained from the particles marked with the number ‘‘1” and ‘‘2” for the three foams.

Fig. S1). A similar characteristic was observed for the PM type foam. Fig. 3e reveals oxide layer wrinkles in unetched condition. Etching process removed the oxide layer/wrinkles, thus revealing particles lying underneath the oxide layer (Fig. 3f). These particles could be $MgAl_2O_4$ or MgO or SiO_2 as suggested by the XRD analysis of the extracted particles from PM foam (details of the analysis are pro- vided in the Supplementary material, Fig. S2). In both Alporas and PM foams, the particles are only few in number. In the entire analy- sis, the reported non-stoichiometry of the particle compositions is due to the volumetric interactions of the electron beam with the aluminium matrix beneath the targeted particles during EDS analysis. For the partially and fully hidden particles, etching process facilitates a more accurate analysis (by EDS), which is otherwise affected by an oxide layer cover. The etchant first comes in contact with the gas-solid interfacial alumina layer and therefore dissolves it first. Once the alumina layer is removed, it may also dissolve the alumina particles partially depending on the duration of exposer. A longer exposer can reduce the particle size significantly. That is why the etching was performed for a short duration (~10 s). Note that, this technique may not be suitable for revealing nanometer-sized particles as these particles may dissolve during the process. The etching technique followed here – sample immersion keeping the reacting surface facing downward and gentle shaking – ensures that the reaction products go into the etchant solution and do not deposit on the etched surface instead. Visualisation of the interfacial particles is imperative to understand whether or not the particles play an important role in stabilisation of the foam. For example, a significant particle coverage at the gas-solid interface in MIT and Alcan type foams implies that surface coverage is an important factor in the sta- bilisation for these foams [1,3]. On the hand, particle coverage does not play a crucial role in the stabilisation of Alporas and PM foams. Once the particles are made visible, quantitative information on surface coverage can be obtained by employing simple

image analysis. A demonstration of this is provided in the Supplementary information, Fig. S3. MIT_Al foam has about 17% (obtained by analysing five SEM images) surface coverage by alumina particles. Since etching can reveal the particles over a large surface area, a large sample size can be analysed. In this way, a reliable statistic can be obtained on the surface coverage as opposed to other techniques which can analyse only a small sample size.

4. Summary

Metallographic etching was used to reveal the particles at the gas-solid interface of different types of aluminium foams. This technique is useful especially when the gas-solid interface of a foam is covered by an oxide layer that fully or partially hides the stabilising particles. This technique is easy-to-perform and suitable for a large sample size. Crucial information such as particle coverage can be obtained by applying the etching technique.

Credit authorship contribution statement:

V. Pamidi: . G. Mohan Muralikrishna: Investigation. S. Bhogi:
Resources, Investigation. K. Georgy: Resources, Investigation.
B. Muduli: Resources, Investigation. F. García-Moreno: Resources, Writing - review & editing. M. Mukherjee:

Appendix A. Supplementary data

Supplementary data to this article can be found online at https://doi.org/10.1016/j.matlet.2020.128371.

References

[1] S.W. Ip, Y. Wang, J.M. Toguri, Can. Metall. Q. 38 (1999) 81–92.
[2] S. Bhogi, J. Nampoothiri, K.R. Ravi, M. Mukherjee, Mater. Sci. Eng. A 685 (2017) 131–138.
[3] N. Babcsán, D. Leitlmeier, H.P. Degischer, J. Banhart, Adv. Eng. Mater. 6 (2004) 421–428.
[4] C. Körner, M. Arnold, R.F. Singer, Mater. Sci. Eng. A 396 (2005) 28–40.
[5] A. Dudka, F. García-Moreno, N. Wanderka, J. Banhart, Acta Mater. 56 (2008) 3990–4001.
[6] S. Bhogi, M. Mukherjee, Mater. Lett. 200 (2017) 118–120.
[7] H. Kumagai, Y. Torikata, H. Yoshimura, M. Kato, T. Yano, Agric. Biol. Chem. 55 (1991) 1823–1829.
[8] F. García-Moreno, S.T. Tobin, M. Mukherjee, C. Jiménez, E. Solórzano, G.S. Vinod Kumar, S. Hutzler, J. Banhart, Soft Matter 10 (2014) 6955–6962.
[9] A. Haibel, A. Rack, J. Banhart, Appl. Phy. Lett. 89 (2006) 154102.
[10] K. Heim, G.S. Vinod Kumar, F. García-Moreno, A. Rack, J. Banhart, Acta Mater. 99 (2015) 313–324.
[11] G.S. Vinod Kumar, M. Chakraborty, F. García-Moreno, J. Banhart, Metall. Mater. Trans. A 42 (2011) 2898–2908.
[12] V. Pamidi, M. Mukherjee, Materialia 4 (2018) 500–509.
[13] V. Pamidi, M. Mukherjee, Trans. Indian Inst. Met. 73 (2020) 191–198.
[14] T. Miyoshi, M. Itoh, S. Akiyama, A. Kitahara, Adv. Eng. Mater. 2 (2000) 179–183. [15] B. Muduli, T. Ramesh, K.C. Hari Kumar, N. Rajalakshmi, M. Mukherjee, Materialia 8 (2019) 100431.
[16] M. Mohammadtaheri, Metallogr. Microstruct. Anal. 1 (2012) 224–226.